Progress of Theoretical Physics, Vol. 125, No. 6, June 2011

Nucleon-Nucleon Potential and Its Non-Locality in Lattice QCD

Keiko MURANO,[1,*)] Noriyoshi ISHII,[2] Sinya AOKI[2,3] and Tetsuo HATSUDA[4,5]

[1]*KEK Theory Center, Institute of Particle and Nuclear Studies, High Energy Accelerator Research Organization (KEK), Tsukuba 305-0801, Japan*
[2]*Graduate School of Pure and Applied Sciences, University of Tsukuba, Tsukuba 305-8571, Japan*
[3]*Center for Computational Sciences, University of Tsukuba, Tsukuba 305-8577, Japan*
[4]*Department of Physics, The University of Tokyo, Tokyo 113-0033, Japan*
[5]*Institute for the Physics and Mathematics of the Universe (IPMU), The University of Tokyo, Kashiwa 277-8583, Japan*

(Received March 2, 2011; Revised April 10, 2011)

By the quenched lattice QCD simulation for two nucleons with finite scattering energy, validity of the derivative expansion of the general nucleon-nucleon potential $U(\boldsymbol{r},\boldsymbol{r}') = V(\boldsymbol{r},\nabla_{\boldsymbol{r}})\delta^3(\boldsymbol{r}-\boldsymbol{r}')$ is studied. The relative kinetic energy between two nucleons is introduced through the anti-periodic boundary condition in the spatial directions. On a hypercubic lattice with the lattice spacing $a \simeq 0.137$ fm and the spatial extent $L_{\rm s} \simeq 4.4$ fm with the pion mass $m_\pi \simeq 530$ MeV, the local potentials for two different energies ($E \simeq 0$ MeV and 45 MeV) are compared and found to be identical within statistical errors, which validates the local approximation of $U(\boldsymbol{r},\boldsymbol{r})$ up to $E = 45$ MeV for the central and tensor potentials. Central potentials in the spin-singlet channel for different orbital angular momentums ($\ell = 0$ and $\ell = 2$) at $E \simeq 45$ MeV are also found to be the same within the errors, which also supports the local approximation.

Subject Index: 234

§1. Introduction

The nucleon-nucleon (NN) potential[1)–3)] is a fundamental quantity to study various properties of atomic nuclei and nuclear matter. Recently, a first attempt to calculate the NN potential from QCD was reported on the basis of the Nambu-Bethe-Salpeter (NBS) wave function for the two nucleons on the lattice.[4),5)] Also, the method has been extended to the baryon-baryon (BB) interactions with strangeness,[6)–8)] the three-nucleon interaction[9)] and meson-baryon interactions.[10),11)] Since the NN interaction is short ranged, the NN potential extracted from lattice QCD simulations is exponentially insensitive to the spatial lattice extent $L_{\rm s}$ as long as $L_{\rm s} \gg 1/m_\pi$. Then one can calculate observables such as the scattering phase shifts by employing the lattice NN potential and solving the Schrödinger equation in the infinite volume.

In general, the lattice NN potential obtained from the NBS wave function is energy-independent but non-local, $U(\boldsymbol{r},\boldsymbol{r}')$. In practice, U is rewritten in terms of

*) Address after April 1st, 2011: RIKEN Nishina Center, RIKEN, Wako 351-0198, Japan

an infinite set of energy-independent local potentials $V^{(\mathrm{LO})}(\boldsymbol{r})$, $V^{(\mathrm{NLO})}(\boldsymbol{r}), \cdots$, by the derivative expansion. These local potentials are determined successively by measuring the NBS wave functions for different scattering energies E below the inelastic threshold E_{th}. A possible criterion for the validity of the derivative expansion at low energies is the stability of the local potentials against the variation of the scattering energy in the interval $0 \leq E < E_{\mathrm{th}}$.*)

The purpose of this paper is to check such stability through the lattice data at $E \simeq 0$ MeV and $E \simeq 45$ MeV: these two cases are realized on the lattice by taking the periodic and anti-periodic boundary conditions in the spatial directions. We carry out quenched lattice QCD simulations with $L_{\mathrm{s}} \simeq 4$ fm and the pion mass $m_\pi \simeq 530$ MeV. We will show that the leading-order local potentials at the above two different energies show no difference within statistical error, which validates the local approximation up to $E = 45$ MeV for the central and tensor potentials.**) Difference of the spin-singlet central potentials between $\ell = 0$ and $\ell = 2$ is also studied, with ℓ being the orbital angular momentum. A preliminary account of these results is given in Refs. 13) and 14).

This paper is organized as follows. In §2, we make a brief review on the energy-independent non-local potential and its derivative expansion. An explicit construction of the leading order terms of the derivative expansion is also presented. In §3, we explain a method to realize non-zero energy NN scattering on the lattice through the spatial boundary conditions. In particular, we introduce a novel momentum wall source operators which are suitable for the purpose of the present paper. In §4, we present numerical results for the NBS wave functions and the associated leading order potentials for different E and ℓ. Section 5 is devoted to a summary and concluding remarks. In Appendix A, we give a brief summary of the representation of the cubic group used in this paper. In Appendix B, some details of constructing the $\ell = 2$ source operator by using the cubic group representation are presented.

§2. Non-local NN potential and its derivative expansion

To define the NN potential in QCD, we consider the equal-time Nambu-Bethe-Salpeter (NBS) wave function in the center of mass (CM) frame defined by

$$\phi_{\alpha\beta}(\boldsymbol{r}; k) \equiv \langle 0 | p_\alpha(\boldsymbol{x}) n_\beta(\boldsymbol{y}) | B = 2; k \rangle, \qquad (\boldsymbol{r} \equiv \boldsymbol{x} - \boldsymbol{y}) \tag{2·1}$$

where $|B = 2; k\rangle$ is a QCD eigenstate with baryon number two ($B = 2$), and $p_\alpha(x)$, $n_\beta(y)$ are local composite nucleon operators with spinor indices α and β. The asymptotic relative momentum k is related to the relativistic total energy W as $W = 2\sqrt{m_N^2 + k^2}$ with m_N being the nucleon mass. In the following, we consider the elastic region where $W < W_{\mathrm{th}} \equiv 2m_N + m_\pi$ is satisfied with the pion mass m_π.

The asymptotic behavior of the NBS wave function for $|\boldsymbol{r}| > R$ (R being the typi-

*) Note that E_{th} is an observable determined by the pion mass and is considerably smaller than the scale of the lattice cutoff a^{-1}.

**) In Ising field theory, it is analytically shown that the energy-dependence is weak at low energy, indicating that the non-locality of the potential is weak.[12)]

cal interaction range) is characterized by the scattering phase shift for hadrons.[5),15)–19)] On the other hand, from the NBS wave function for $|\boldsymbol{r}| < R$, we can define a k-dependent local potential $U_k(\boldsymbol{r})$ and derive an associated k-independent non-local potential $U(\boldsymbol{r}, \boldsymbol{r}')$ with the use of the information of the NBS wave functions for $E < E_{\rm th}$:

$$\left(\nabla_{\boldsymbol{r}}^2 + k^2\right)\ \phi(\boldsymbol{r}; k) \equiv 2\mu U_k(\boldsymbol{r})\phi(\boldsymbol{r}; k) \tag{2·2}$$

$$= 2\mu \int d^3r'\ U(\boldsymbol{r}, \boldsymbol{r}')\ \phi(\boldsymbol{r}'; k), \tag{2·3}$$

where $\mu = m_N/2$ denotes the reduced mass of the NN system. Derivation of Eq. (2·3) from Eq. (2·2) is given explicitly in Ref. 5). Note also that an equivalence theorem between $U_k(\boldsymbol{r})$ and $U(\boldsymbol{r}, \boldsymbol{r}')$ has been proved in a different manner in Ref. 20). In practical applications, $U(\boldsymbol{r}, \boldsymbol{r}')$ has advantages over $U_k(\boldsymbol{r})$; its k-independence leads to the standard eigenvalue problem for the NBS wave function. Furthermore its non-locality can be treated by the derivative expansion, $U(\boldsymbol{r}, \boldsymbol{r}') = V(\boldsymbol{r}, \nabla_{\boldsymbol{r}})\delta^3(\boldsymbol{r} - \boldsymbol{r}')$, with

$$V(\boldsymbol{r}, \nabla_{\boldsymbol{r}}) = \underbrace{V_0(r) + V_\sigma(r)(\boldsymbol{\sigma}_1 \cdot \boldsymbol{\sigma}_2) + V_{\rm T}(r)S_{12}}_{\rm LO} + \underbrace{V_{\rm LS}(r)\ \boldsymbol{L}\cdot\boldsymbol{S}}_{\rm NLO} + \mathcal{O}(\nabla^2), \tag{2·4}$$

where $S_{12} \equiv 3(\boldsymbol{\sigma}_1\cdot\boldsymbol{r})(\boldsymbol{\sigma}_2\cdot\boldsymbol{r})/r^2 - \boldsymbol{\sigma}_1\cdot\boldsymbol{\sigma}_2$, $\boldsymbol{S} \equiv (\boldsymbol{\sigma}_1 + \boldsymbol{\sigma}_2)/2$ and $\boldsymbol{L} \equiv \boldsymbol{r}\times(-i\nabla_{\boldsymbol{r}})$ denote the tensor operator, the total spin operator and the orbital angular momentum operator, respectively.[21),22)]

Since the total wave function has to be anti-symmetric under the exchange of two nucleons, possible combinations of the total isospin I, the total spin S and the orbital angular momentum ℓ are restricted to four cases, (I, S, ℓ)=(1,0,even), (0,1,even), (1,1,odd) and (0,0,odd). Thus we may omit the isospin I indices in Eq. (2·4). Note that the spin-singlet states ($S = 0$) and spin-triplet states ($S = 1$) do not mix with each other, since the isospin I and the parity $P = (-1)^\ell$ are conserved for QCD with degenerate 2-flavors. To specify two-nucleon scattering states, we follow the standard notation, ${}^{2S+1}\ell_J$, with J being the total angular momentum.

2.1. *Spin-singlet potentials*

Let us first consider the spin-singlet channel. Since contributions from S_{12} and $\boldsymbol{L}\cdot\boldsymbol{S}$ terms are absent in this case, the Schrödinger equation reads

$$\left(\nabla_{\boldsymbol{r}}^2 + k^2\right)\phi(\boldsymbol{r}; k) = 2\mu\left[V_0(r) - 3V_\sigma(r) + \left\{\nabla_{\boldsymbol{r}}^2, V_{p^2}(r)\right\} + V_{L^2}(r)\boldsymbol{L}^2 + \mathcal{O}(\nabla^4)\right]\phi(\boldsymbol{r}; k). \tag{2·5}$$

Terms involving $2n$ derivatives such as $(\boldsymbol{L}^2)^n$ and $(\nabla^2)^n$ give N^{2n}LO potentials. (Note that N^{2n+1}LO potentials are absent in the spin-singlet channel.) At the LO level, the Schrödinger equation (2·5) reduces to

$$\left(\nabla_{\boldsymbol{r}}^2 + k^2\right)\phi(\boldsymbol{r}; k) = 2\mu V_{\rm C,s}^{\rm (LO)}(r)\phi(\boldsymbol{r}; k), \tag{2·6}$$

with $V_{\rm C,s}^{\rm (LO)}(r) \equiv V_0(r) - 3V_\sigma(r)$. Then the LO central potential in the spin-singlet channel is given by

$$V_{\rm C,s}^{\rm (LO)}(r) \equiv E + \frac{1}{2\mu}\frac{\nabla_{\boldsymbol{r}}^2 \phi(\boldsymbol{r};k)}{\phi(\boldsymbol{r};k)}, \tag{2·7}$$

where $E \equiv \frac{k^2}{2\mu}$ is the effective kinetic energy between two nucleons. The above LO truncation works only when the right-hand side of Eq. (2·7) depends weakly on k and ℓ. This will be checked explicitly in §4 at low energies and at low angular momentums through the comparisons, ($\ell = 0, E \simeq 0$ MeV) vs ($\ell = 0, E \simeq 45$ MeV) and ($\ell = 0, E \simeq 45$ MeV) vs ($\ell = 2, E \simeq 45$ MeV).

If k and ℓ dependence in the spin-singlet channel becomes visible as these values increase, it is a sign of the NNLO terms in Eq. (2·5). Then the next step is to determine NNLO potentials $V_{\rm C,s}^{\rm (NNLO)}(r)$, $V_{p^2}^{\rm (NNLO)}(r)$ and $V_{L^2}^{\rm (NNLO)}(r)$ through the NBS wave functions measured with three different combinations of k and ℓ. Such a procedure continues to higher orders as k and ℓ further increase. A close analogy of this process is the renormalization-scale (κ) dependence in the perturvative series of quantum field theory; the artificial κ dependence of scale-independent quantities is canceled order by order as we proceed to higher orders.

2.2. *Spin-triplet potentials*

For the spin-triplet channel, the Schrödinger equation reads

$$\left(\nabla_{\boldsymbol{r}}^2 + k^2\right)\phi(\boldsymbol{r};k) = 2\mu\left[V_0(r) + V_\sigma(r) + V_{\rm T}(r)S_{12} + V_{\rm LS}(r)\boldsymbol{L}\cdot\boldsymbol{S} + \mathcal{O}(\nabla^2)\right]\phi(\boldsymbol{r};k). \tag{2·8}$$

At the LO level, it reduces to

$$\left(\nabla_{\boldsymbol{r}}^2 + k^2\right)\phi(\boldsymbol{r};k) = 2\mu\left[V_{\rm C,t}^{\rm (LO)}(r) + V_{\rm T}^{\rm (LO)}(r)S_{12}\right]\phi(\boldsymbol{r};k), \tag{2·9}$$

where $V_{\rm C,t}^{\rm (LO)}(r) \equiv V_0(r) + V_\sigma(r)$.

To be specific, we restrict ourselves to the case with $J^P = 1^+$ NBS wave function to which two partial waves contribute, i.e., ${}^3{\rm S}_1$ (S-wave [$\ell = 0$]) and ${}^3{\rm D}_1$ (D-wave [$\ell = 2$]). As shown in Ref. 5), Eq. (2·9) consists of two independent equations

$$\begin{pmatrix} \mathcal{P}\phi(\boldsymbol{r};k) & \mathcal{P}S_{12}\phi(\boldsymbol{r};k) \\ \mathcal{Q}\phi(\boldsymbol{r};k) & \mathcal{Q}S_{12}\phi(\boldsymbol{r};k) \end{pmatrix}\begin{pmatrix} V_{\rm C,t}^{\rm (LO)}(r) - k^2/2\mu \\ V_{\rm T}^{\rm (LO)}(r) \end{pmatrix} = \frac{\nabla_{\boldsymbol{r}}^2}{2\mu}\begin{pmatrix} \mathcal{P}\phi(\boldsymbol{r};k) \\ \mathcal{Q}\phi(\boldsymbol{r};k) \end{pmatrix}, \tag{2·10}$$

where $\mathcal{P}$ ($\mathcal{Q}$) is a projection to the $\ell = 0$ ($\ell = 2$) state. The LO potentials, $V_{\rm C,t}^{\rm (LO)}(r)$ and $V_{\rm T}^{\rm (LO)}(r)$, are obtained by solving this 2×2 matrix equation algebraically.

Spatial symmetry group of the hyper-cubic lattice is the cubic transformation group $SO(3,\mathbb{Z})$ instead of the rotation group $SO(3,\mathbb{R})$. Here we employ the $J^P = T_1^+$ representation of the $SO(3,\mathbb{Z})$ for the wave function in the spin-triplet channel.*) Since the spin-triplet belongs to the T_1 representation, the $J^P = T_1^+$ state in general

*) Here J is used to represent the quantum number of orbital $\otimes$ spin even for the discrete group $SO(3,\mathbb{Z})$, and P is the parity under the spatial reflection.

contains orbital state R which satisfies $T_1^+ \in R \otimes T_1$. Table II in Appendix A.1 gives $R = A_1^+$, E^+, T_2^+ and T_1^+. Among them we take the projection to the orbital A_1^+ representation for $\mathcal{P}$ as

$$\mathcal{P}\phi(\boldsymbol{r};k) \equiv \frac{1}{24}\sum_{\mathcal{R}\in SO(3,\mathbb{Z})} \phi(\mathcal{R}^{-1}[\boldsymbol{r}];k), \tag{2·11}$$

where the summation is performed over the cubic group $SO(3,\mathbb{Z})$ with 24 elements. The orbital A_1 representation is expected to be dominated by the S-wave up to contamination of higher partial waves with $\ell \geq 4$. We employ $\mathcal{Q} = 1 - \mathcal{P}$ as a projection to non-A_1^+ orbital components composed of E^+, T_2^+ and T_1^+ representations. Non-A_1^+ orbital components are expected to be dominated by the D-wave up to contamination of higher partial waves with $\ell \geq 4$. Note that E^+ and T_2^+ contain the $\ell = 2$ component, whereas T_1^+ does not contain the $\ell = 2$ component.

If k and ℓ dependence in the spin-triplet channel becomes visible as these values increase, it is a sign of the NLO terms in Eq. (2·8). Then the next step is to determine NLO potentials through the NBS wave functions measured with several different combinations of k and ℓ.

§3. Finite-energy NN scattering on the lattice

To extract the NBS wave function on the lattice, we start with the four-point nucleon correlation function,

$$G_{\alpha\beta}(\boldsymbol{x}-\boldsymbol{y},t-t_0;\mathcal{J}_{pn}) \equiv \frac{1}{L_{\rm s}^3}\sum_{\boldsymbol{r}}\langle 0|T[p_\alpha(\boldsymbol{x}+\boldsymbol{r},t)n_\beta(\boldsymbol{y}+\boldsymbol{r},t)\mathcal{J}(t_0)]|0\rangle, \tag{3·1}$$

$$\simeq \ \phi_{\alpha\beta}(\boldsymbol{x}-\boldsymbol{y};k)\langle B=2;k|\mathcal{J}(0)|0\rangle e^{-W(t-t_0)}, \quad t-t_0 \gg 1, \tag{3·2}$$

where the summation over $\boldsymbol{r}$ is performed to select the two nucleon system with total spatial momentum zero, $\mathcal{J}(t_0)$ denotes a two-nucleon source located at $t = t_0$, whose explicit form will be specified below. The relativistic energy and associated asymptotic momentum of the "ground" state of the $B = 2$ system are denoted by W and k, respectively. As for the sink operators, $p(x)$ and $n(x)$, we employ the following local composite operators,

$$p(x) \equiv \epsilon_{abc}\left(u_a^T(x)C\gamma_5 d_b(x)\right)u_c(x), \qquad n(x) \equiv \epsilon_{abc}\left(u_a^T(x)C\gamma_5 d_b(x)\right)d_c(x), \tag{3·3}$$

where a, b, c are color indices.

The NBS wave function at $E \simeq 0$ MeV is generated under the periodic boundary condition (PBC), which is imposed on the quark operators along the spatial directions. With the PBC, the momentum of a single nucleon is discretized as $k_i = 2\pi n_i/L_{\rm s}$ with $n_i \in \mathbb{Z}$. Hence, the lowest lying state of the two nucleon system in the CM frame roughly corresponds to the state where two nucleons are weakly interacting with relative momentum of $k_i \simeq 0$ MeV. The effective kinetic energy of such a state is $E \equiv k^2/m_N \simeq 0$ MeV. The NBS wave function at $E \simeq 45$ MeV is generated under the anti-periodic boundary condition (APBC). Since the nucleon

also obeys the APBC, the spatial momentum of a single nucleon is discretized as $k_i = (2n_i+1)\pi/L_{\rm s}$ with $n_i \in \mathbb{Z}$. Hence, the lowest lying state of the two nucleon system in the CM frame roughly corresponds to the state where two nucleons are weakly interacting with relative momentum of $k_i \simeq \pm\pi/L_{\rm s}$. For the lowest lying state with $L_{\rm s} \simeq 4.4$ fm, the spatial momentum of a nucleon amounts to $|\boldsymbol{k}| \simeq \sqrt{3}\pi/L_{\rm s} \simeq 245$ MeV, which corresponds to $E \simeq 45$ MeV in our setup with $m_N \simeq 1.33$ GeV.

As for the source operators of the two nucleon system, we employ

$$\mathcal{J}_{\alpha\beta}(f) \equiv \bar{P}_\alpha(f)\bar{N}_\beta(f), \tag{3·4}$$

where $\bar{P}_\alpha(f)$ and $\bar{N}_\beta(f)$ associated with a source function $f(\boldsymbol{x})$ are given as

$$\begin{aligned} \bar{P}(f) &\equiv \epsilon_{abc}\left(\bar{U}_a(f)C\gamma_5\bar{D}_b^T(f)\right)\bar{U}_c(f), \\ \bar{N}(f) &\equiv \epsilon_{abc}\left(\bar{U}_a(f)C\gamma_5\bar{D}_b^T(f)\right)\bar{D}_c(f). \end{aligned} \tag{3·5}$$

Here the source operators for u and d quarks are given by

$$\bar{U}(f) \equiv \sum_{\boldsymbol{x}} \bar{u}(\boldsymbol{x})f(\boldsymbol{x}), \qquad \bar{D}(f) \equiv \sum_{\boldsymbol{x}} \bar{d}(\boldsymbol{x})f(\boldsymbol{x}). \tag{3·6}$$

An element $\mathcal{R}$ of the cubic group $SO(3,\mathbb{Z})$ rotates the quark field operator as

$$\bar{q}(\boldsymbol{x}) \mapsto \bar{q}(\mathcal{R}^{-1}\boldsymbol{x})\Lambda(\mathcal{R}^{-1}), \tag{3·7}$$

where Λ denotes the 4-component spinor representation of O as $\Lambda(e^\omega) \equiv \exp\left(-\frac{i}{4}\sigma_{ij}\omega^{ij}\right)$ with $\sigma_{\mu\nu} \equiv \frac{i}{2}[\gamma_\mu, \gamma_\nu]$. This leads to the transformation property of $\mathcal{J}_{\alpha\beta}(f)$ as

$$\mathcal{J}_{\alpha\beta}(f) \mapsto \mathcal{J}_{\alpha'\beta'}(\mathcal{R}^{-1}\circ f)\Lambda_{\alpha'\alpha}(\mathcal{R}^{-1})\Lambda_{\beta'\beta}(\mathcal{R}^{-1}), \tag{3·8}$$

where $(\mathcal{R}^{-1}\circ f)(\boldsymbol{x}) \equiv f(\mathcal{R}\boldsymbol{x})$.

To consider $J = 0$ and 1, it is convenient to introduce a source operator which has definite J and M with $J = 0 + S$ and $M = 0 + S_z$ to construct NBS wave functions in the ${}^1\mathrm{S}_0$ and ${}^3\mathrm{S}_1 - {}^3\mathrm{D}_1$ channels:

$$\mathcal{J}^{(J,M)}(f) \equiv \frac{1}{24}\sum_{\mathcal{R}\in SO(3,\mathbb{Z})} \mathcal{J}_{\alpha\beta}(\mathcal{R}^{-1}\circ f)\cdot P_{\alpha\beta}^{(S=J,S_z=M)}, \tag{3·9}$$

where $P_{\alpha\beta}^{(S,S_z)}$ denotes the spin projection operator defined as $P_{\alpha\beta}^{(S=0,S_z=0)} \equiv (\sigma_2)_{\alpha\beta}/\sqrt{2}$, $P_{\alpha\beta}^{(S=1,S_z=M)} \equiv (\sigma_2\sigma_M)_{\alpha\beta}/\sqrt{2}$ with $M = \pm1, 0$, where we take only the upper components of the Dirac indices for simplicity.

For the PBC, we employ a flat wall (f-wall) source,

$$f^{(\text{f-wall})}(\boldsymbol{r}) = 1, \tag{3·10}$$

which is invariant under the rotation $\mathcal{R}$. Then, Eq. (3·9) reduces to

$$\mathcal{J}^{(J,M)}(f^{(\text{f-wall})}) = \bar{P}_\alpha(f^{(\text{f-wall})})\bar{N}_\beta(f^{(\text{f-wall})})\cdot P_{\alpha\beta}^{(S=J,S_z=M)}, \tag{3·11}$$

which couples dominantly to the ground state ($\boldsymbol{k} = (0,0,0)\pi/L_{\rm s}$) in the PBC.

For the APBC, we utilize a set of momentum wall sources $f^{(\text{m-wall})} = \{f^{(i)}\}_{i=0-3}$ with

$$\begin{aligned} f^{(0)}(\boldsymbol{r}) &\equiv \cos((+x+y+z)\pi/L_{\text{s}}), \\ f^{(1)}(\boldsymbol{r}) &\equiv \cos((-x+y+z)\pi/L_{\text{s}}), \\ f^{(2)}(\boldsymbol{r}) &\equiv \cos((-x-y+z)\pi/L_{\text{s}}), \\ f^{(3)}(\boldsymbol{r}) &\equiv \cos((+x-y+z)\pi/L_{\text{s}}), \end{aligned} \tag{3·12}$$

where the cosine function is chosen to create positive parity states.

The cubic group acts on these functions as permutation, which is characterized by the cubic group representation, $A_1^+ \oplus T_2^+$. By taking the A_1^+ part, Eq. (3·9) becomes

$$\mathcal{J}^{(J,M)}(f^{(\text{m-wall})}; A_1^+) \equiv \frac{1}{4}\sum_{j=0}^{3} \bar{P}_\alpha(f^{(j)})\bar{N}_\beta(f^{(j)}) \cdot P_{\alpha\beta}^{(S=J,S_z=M)}, \tag{3·13}$$

which couples dominantly to the ground state ($\boldsymbol{k} = (1,1,1)\pi/L_{\text{s}}$) in the APBC. Since this source operator is not translational invariant, it is practically important to perform a summation over $\boldsymbol{r}$ at the sink side in Eq. (3·1) to pick up zero spatial momentum states. Instead of Eq. (3·12), one may choose a simpler cosine-type function

$$f(\boldsymbol{r}) \equiv \cos(\pi x/L_{\text{s}})\cos(\pi y/L_{\text{s}})\cos(\pi z/L_{\text{s}}), \tag{3·14}$$

which gives a source operator coupled to the ground state ($\boldsymbol{k} = (1,1,1)\pi/L_{\text{s}}$) in the APBC. However, it receives a contamination from the coupling with the first excited state ($\boldsymbol{k} = (3,1,1)\pi/L_{\text{s}}$). In contrast, the source operator with Eq. (3·12) has an overlap neither with the first excited state nor the second excited state, and receives contamination only from the third excited state ($\boldsymbol{k} = (3,3,3)\pi/L_{\text{s}}$). Therefore, signal for the ground state is better for Eq. (3·12) than that for Eq. (3·14).

Since Eq. (3·12) contains T_2^+ component, it can be also used to generate the state in the ${}^1\text{D}_2$ channel, which is employed to study the ℓ dependence of $V_{\text{C,s}}^{(\text{LO})}(r)$. A general projection formula for the source operator in the spin-singlet sector given in Eq. (B·1) leads to

$$\mathcal{J}^{(J=2,M)}(f^{(\text{m-wall})}; T_2^+) = \frac{1}{4}\sum_{j=0}^{3} e^{iMj\pi/2}\bar{P}_\alpha(f^{(j)})\bar{N}_\beta(f^{(j)}) \cdot P_{\alpha\beta}^{(S=0,S_z=0)} \tag{3·15}$$

for the T_2^+ representation, where M takes 2 and ± 1 (modulo 4). See Appendices B and A.2 for more details. In the actual numerical calculation, we take linear combinations of Eq. (3·15) to make them into real basis as

$$\begin{aligned} \mathcal{J}^{J=2,xy} &\equiv \mathcal{J}^{J=2,M=2}, \\ \mathcal{J}^{J=2,yz} &\equiv \frac{i}{\sqrt{2}}\left(\mathcal{J}^{J=2,M=-1} + \mathcal{J}^{J=2,M=1}\right), \\ \mathcal{J}^{J=2,zx} &\equiv \frac{1}{\sqrt{2}}\left(\mathcal{J}^{J=2,M=-1} - \mathcal{J}^{J=2,M=1}\right). \end{aligned} \tag{3·16}$$

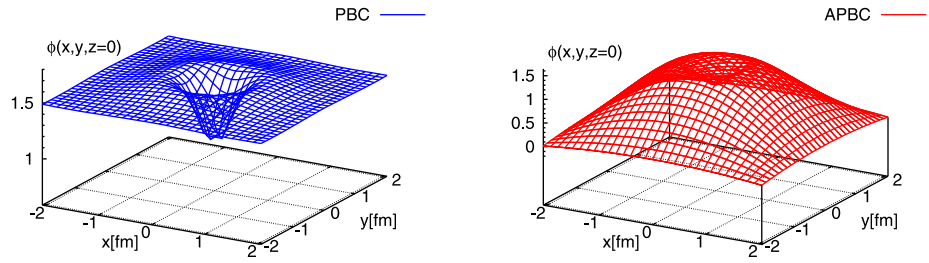

Fig. 1. (Left) The NBS wave function for the spin-singlet and the orbital A_1^+ channel at $E \simeq 0$ MeV with the PBC. (Right) The NBS wave function in the same channel but at $E \simeq 45$ MeV with the APBC. Both wave functions are normalized as $\phi(r = 0) = 1$.

§4. Numerical results

4.1. *Lattice setup*

Employing the standard plaquette gauge action on a $32^3 \times 48$ lattice at $\beta = 5.7$, quenched gauge configurations are generated by the heat-bath algorithm with the over-relaxation. We accumulate 4000 configurations separated by 200 sweeps. The standard Wilson quark action is used to calculate quark propagators with the hopping parameter $\kappa = 0.1665$. The Dirichlet boundary condition in the temporal direction is imposed at $t - t_0 = \pm 24$. The nucleon four-point correlation functions are measured for both $t - t_0 > 0$ and $t - t_0 < 0$ to improve the statistics by using the time-reversal and charge conjugation symmetries.[5] Either PBC or APBC is taken in the spatial direction: In the former case, we use four sources at $t_0 = 0, 8, 16, 24$ to improve the statistics. These calculations are performed on Blue Gene/L at KEK.

From the rho meson mass in the chiral limit, the lattice spacing is determined to be $a^{-1} = 1.44(2)$ GeV ($a \simeq 0.137$ fm), which leads to $L_{\rm s} = 32a \simeq 4.4$ fm. Our κ corresponds to the pion mass $m_\pi \simeq 0.53$ GeV and the nucleon mass $m_N \simeq 1.33$ GeV.[23] After examining the stability of the NN potentials against the variation of $t - t_0$, we chose the wave functions and potentials at $t - t_0 = 9$ in all the plots shown in this paper.

4.2. *The NBS wave functions*

Figure 1 (Left) and (Right) show three dimensional plots of the NBS wave functions $\phi(x, y, z = 0)$ for the spin-singlet and the orbital A_1^+ channel ($\simeq {}^1{\rm S}_0$ channel) at $E \simeq 0$ MeV and at $E \simeq 45$ MeV, respectively. We observe that they behave rather differently: The wave function for the PBC is almost constant at long distances, which indicates that the asymptotic momentum is nearly zero. On the other hand, the wave function for the APBC decreases continuously to zero at long distances, since the wave function in orbital A_1^+ state must vanish on the boundary in APBC. This can be seen, for example, by using a π rotation around the x-axis followed by the spatial reflection as $\phi(x, y, z) = \phi(x, -y, -z) = \phi(-x, y, z) = -\phi(L_{\rm s} - x, y, z)$,

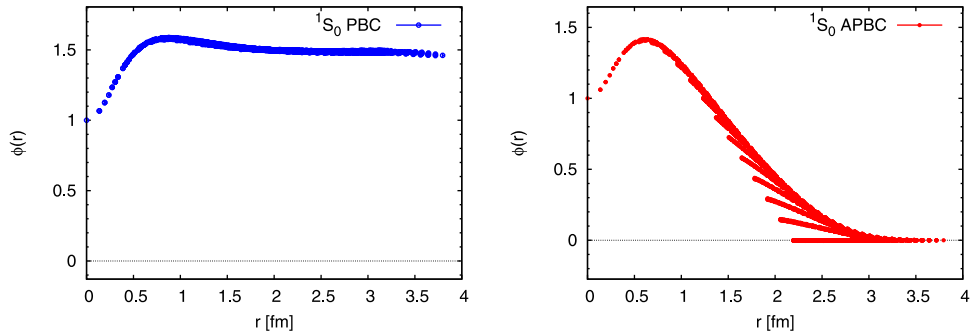

Fig. 2. Same NBS wave functions as in Fig. 1 but as a function of r.

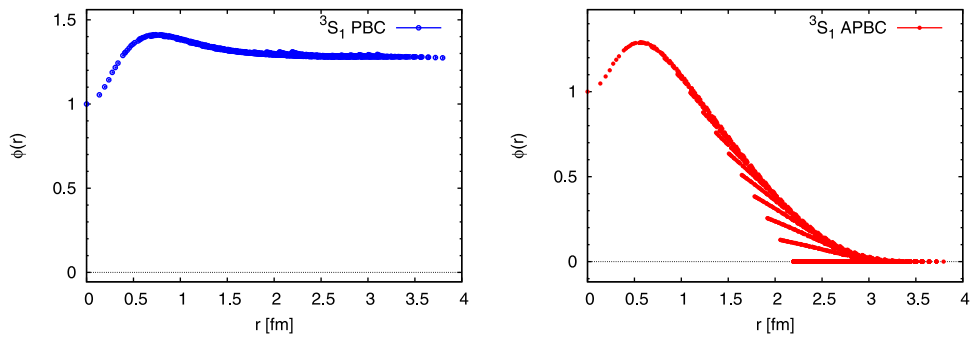

Fig. 3. (Left) The NBS wave function in the spin-triplet and the orbital A_1^+ channel at $E \simeq 0$ MeV with the PBC. (Right) The same at $E \simeq 45$ MeV with the APBC. Both wave functions are normalized as $\phi(r = 0) = 1$.

which leads to $\phi(L_s/2, y, z) = -\phi(L_s/2, y, z) = 0$.

In Fig. 2, the same wave functions as in Fig. 1 are plotted as a function of r. Violation of rotational symmetry due to the square lattice can be seen explicitly through the multi-valuedness of the wave function at large r for the APBC. Shown in Fig. 3 is the similar comparison of NBS wave functions between the PBC and the APBC in the spin-triplet and the orbital A_1^+ channel ($\simeq$ $^3S_1$ channel).

In Fig. 4 (Upper), we plot the NBS wave functions for the spin-triplet and the orbital T_2^+ channel ($\simeq$ $^3D_1$ channel). They are highly multi-valued as functions of r at all distances simply due to the angular dependence of the orbital T_2^+ representation. To extract the radial part only, we divide the wave functions by $Y_{2,m}(\theta, \phi)$ assuming that the angular dependence is dominated by the $\ell = 2$ component. The results are shown in Fig. 4 (Lower): almost single-valued radial wave functions are obtained for both PBC and APBC cases.

4.3. *LO potentials for different energies*

The leading order potentials are extracted from the NBS wave functions according to Eqs. (2·7) and (2·10) for the spin-singlet and spin-triplet channels, respectively. In order to obtain LO potentials, we need to determine the value of $E = k^2/(2\mu)$

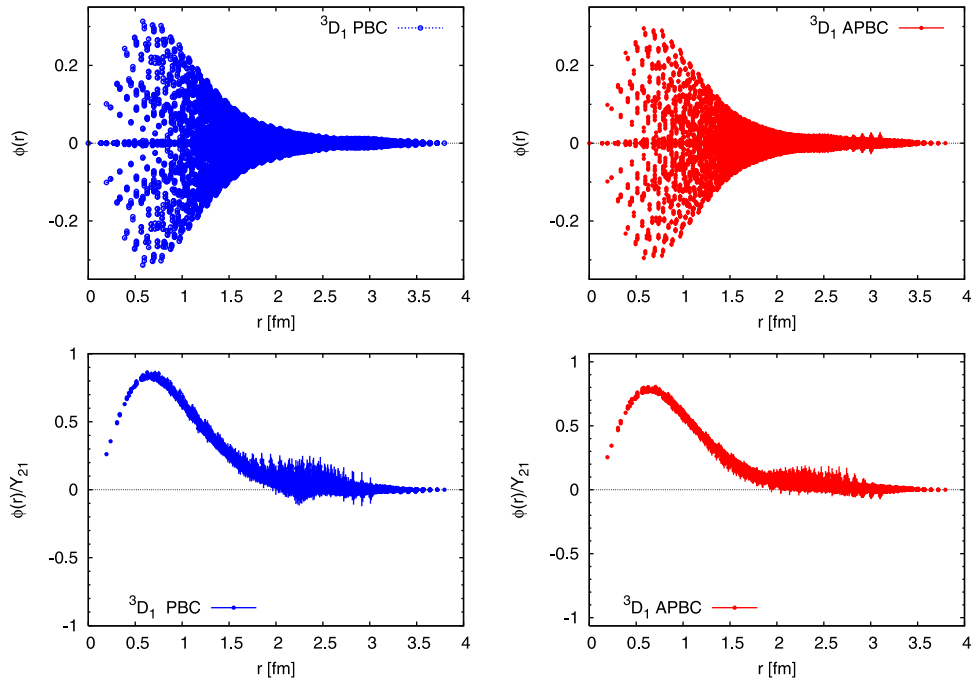

Fig. 4. (Upper-Left) The NBS wave function $\mathrm{Re}\phi_{\downarrow\downarrow}(\boldsymbol{r})$ for the spin-triplet and the orbital T_2^+ channel at $E \simeq 0$ MeV with the PBC. (Upper-Right) The same NBS wave function but at $E \simeq 45$ MeV with the APBC. (Lower-Left) The NBS wave function $\phi_{\downarrow\downarrow}$ divided by the spherical harmonics $Y_{21}(\theta, \phi)$. (Lower-Right) Same as the left figure but at $E \simeq 45$ MeV with the APBC. Normalization of these wave functions is fixed uniquely once the normalization of the S-wave part is fixed as given in Figs. 2 and 3.

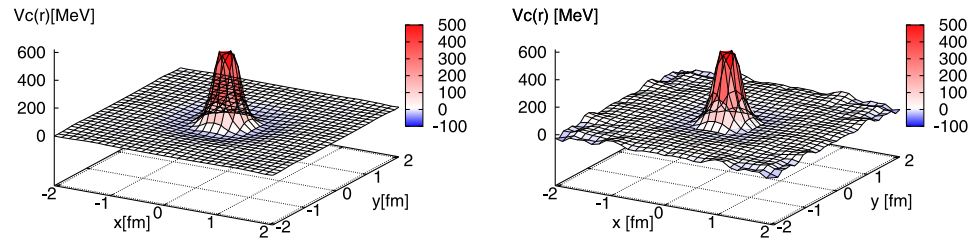

Fig. 5. The spin-singlet central potential, $V_{\mathrm{C,s}}^{\mathrm{LO}}(r)$, (Left) at $E \simeq 0$ MeV and (Right) at $E \simeq 45$ MeV.

either from the large t behavior of the NN correlation function or the large r behavior of the NBS wave function.*) It turns out that the values of E from both determinations are roughly equal to their free values, i.e., $E \simeq 0$ MeV for the PBC

*) We note here that a new method to obtain the potentials by using the t-dependent Schrödinger equation has been also proposed recently.[24]

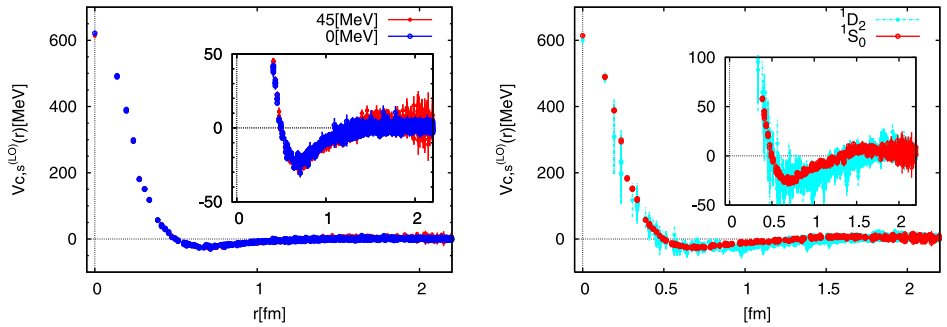

Fig. 6. (color-online)(Left) The LO central potential $V_{\rm C,s}^{\rm (LO)}(r)$ for the spin-singlet and the orbital A_1^+ channel as a function of r at $E \simeq 0$ 45 MeV (red solid circles) and at $E \simeq 0$ MeV (blue open circles). (Right) The LO central potential $V_{\rm C,s}^{\rm (LO)}(r)$ for the spin-singlet channel as a function of r at $E \simeq 45$ MeV, determined from the orbital A_1^+ representation (red open circles) and from the T_2^+ representation (cyan solid circles).

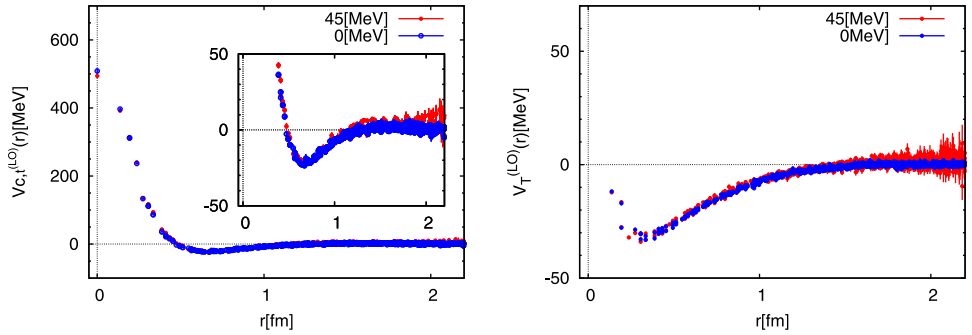

Fig. 7. (Left) The LO central potential $V_{\rm C,t}^{\rm (LO)}(r)$ for the spin-triplet and the orbital ${}^3{\rm S}_1 - {}^3{\rm D}_1$ coupled channel as a function of r. (Right) The LO tensor potential $V_{\rm T}^{\rm (LO)}(r)$ for the spin-triplet and the orbital ${}^3{\rm S}_1 - {}^3{\rm D}_1$ coupled channel as a function of r. Symbols are the same as in Fig. 6.

and $E \simeq 45$ MeV for the APBC, within statistical and systematic errors. Therefore, we adopt these free values as characteristic E in extracting the LO central potentials. Note that the tensor potential is free from the uncertainty of E as can be seen from Eq. (2·10).

In Fig. 5, we plot the spin-singlet central potentials $V_{\rm C,s}^{\rm LO}(x, y, z = 0)$ obtained from the corresponding NBS wave functions $\phi(x, y, z = 0)$ in Fig. 1. Although the wave functions have different spatial structure for different energies, the potentials are independent of E and localized in space.

To make more precise comparison, $V_{\rm C,s}^{\rm (LO)}(r)$ is plotted as a function of r for $E \simeq 0$ MeV (blue open circle) and at $E \simeq 45$ MeV (red closed circle) in Fig. 6 (Left). Similar comparisons are also made for $V_{\rm C,t}^{\rm (LO)}(r)$ and $V_{\rm T}^{\rm (LO)}(r)$ in Fig. 7. In all these cases, we find no E-dependence within statistical errors. We therefore conclude that the LO potential is a good approximation for $U(\boldsymbol{r}, \boldsymbol{r}')$ in the energy range $E = 0$ – 45 MeV.

It should be kept in mind that we employ a large pion mass $m_\pi \simeq 0.53$ GeV, which may be one of the reasons for the small energy dependence of the LO potentials. It is therefore important to increase E or decrease m_π and check the point where NLO contributions become significant.

4.4. *LO potentials for different orbital angular momentum*

As mentioned in §3, source functions in Eq. (3·12) for the APBC generate not only the orbital A_1^+ but also the orbital T_2^+ components. Combining these sources appropriately, one can construct the NBS wave function for the spin-singlet and the orbital T_2^+ channel ($\simeq {}^1\mathrm{D}_2$ state). Therefore the LO central potential $V_{\mathrm{C,s}}^{(\mathrm{LO})}(r)$ can be extracted also from this wave function.

In Fig. 6 (Right), $V_{\mathrm{C,s}}^{(\mathrm{LO})}(r)$ obtained from the orbital T_2^+ channel is compared with the same potential determined from the orbital A_1^+ channel at $E \simeq 45$ MeV. Although statistical errors are large, we observe that the two determinations give consistent result. Assuming that the orbital A_1^+ and T_2^+ representations are dominated by $\ell = 0$ and $\ell = 2$ waves, respectively, we here conclude that the LO potential in the derivative expansion is a good approximation of $U(\boldsymbol{r}, \boldsymbol{r}')$ for $\ell \leq 2$ in the spin-singlet and positive parity channel.

§5. Summary and conclusion

We have studied the validity of derivative expansion of the energy-independent non-local NN potential $U(\boldsymbol{r}, \boldsymbol{r}') = V(\boldsymbol{r}, \nabla_{\boldsymbol{r}})\delta^3(\boldsymbol{r} - \boldsymbol{r}')$, defined from the NBS wave function on the lattice. For this purpose, we have carried out quenched lattice QCD simulations for the NBS wave functions with the lattice spacing 0.14 fm, spatial lattice size 4.4 fm and the pion mass $m_\pi \simeq 530$ MeV. Relative kinetic energies between two nucleons were controlled by employing the periodic and anti-periodic boundary conditions for the quark fields in the spatial directions.

The leading-order potentials obtained at different energies ($E \simeq 0$ MeV and 45 MeV) show no difference within statistical errors, which validates the local approximation of the potential up to $E = 45$ MeV for the central and tensor potentials. We have also compared the central potentials in the spin-singlet channel for different orbital angular momentum ($\ell = 0$ and $\ell = 2$) at $E \simeq 45$ MeV. The result also supports the validity of the local approximation of the potential at this energy.

In the future it is important to apply the analysis in this report to the general baryon-baryon potentials in full QCD for lighter quark masses (smaller inelastic threshold E_{th}) and for smaller lattice spacing a to investigate the convergence of the derivative expansion in realistic situations.

Acknowledgements

We are grateful for authors and maintainers of `CPS++`,[25] a modified version of which is used for simulations done in this report. This work is supported by the Large Scale Simulation Program No. 08-19(FY2008) and No. 09-23(FY2009) of

Table I. Numbers of each representation of $SO(3,\mathbb{Z})$ which appears in the angular momentum ℓ representation of $SO(3,\mathbb{R})$. $P=(-1)^\ell$ represents an eigenvalue under parity transformation.

ℓ	P	A_1	A_2	E	T_1	T_2
0 (S)	+	1	0	0	0	0
1 (P)	−	0	0	0	1	0
2 (D)	+	0	0	1	0	1
3 (F)	−	0	1	0	1	1
4 (G)	+	1	0	1	1	1
5 (H)	−	0	0	1	2	1
6 (I)	+	1	1	1	1	2

High Energy Accelerator Research Organization (KEK). This work was supported in part by the Grants-in-Aid of the Ministry of Education, Science and Technology, Sports and Culture (Nos. 20340047, 20105001, 20105003, 22540268) and in part by a Grand-in-Aid for Specially Promoted Research (13002001).

Appendix A
Spatial Rotation on the Lattice

A.1. *Cubic group $SO(3,\mathbb{Z})$*

In this appendix, we present a brief summary on the symmetry of two nucleon system on the lattice. Further account on the representations of the cubic group can be seen in Refs. 26) and 27). Note that the NBS wave functions in higher partial waves on the lattice are first discussed by Lüscher.[16)]

A relation of irreducible representations between $SO(3,\mathbb{Z})$ and $SO(3,\mathbb{R})$ is given in Table I for $\ell \leq 6$. For two nucleon, the total spin S becomes $1/2 \otimes 1/2 = 1 \oplus 0$, which corresponds to $T_1(S=1)$ and $A_1(S=0)$ of the $SO(3,\mathbb{Z})$. Therefore, the total representation J for two nucleon system is determined by the product $J = R_1 \otimes R_2$, where $R_1 = A_1, A_2, E, T_1, T_2$ for the orbital "angular momentum" while $R_2 = A_1, T_1$ for the total spin. In Table II, the product $R_1 \otimes R_2$ is decomposed into the direct sum of irreducible representations. For example, if the two nucleon state in the spin-triplet ($R_2 = T_1$) belongs to the $J^P = T_1^+$ representation, the orbital representation R_1 should satisfy $T_1^+ \in (R_1 \otimes T_1)$. From Table II, solutions to this condition are given by $R_1 = A_1^+$, E^+, T_1^+ and T_2^+.

A.2. *The cyclic group C_4*

Elements of $SO(3,\mathbb{Z})$ which correspond to the rotation around the z-axis form a cyclic group C_4 consisting of four elements

$$C_4 \equiv \{e, c_4, (c_4)^2, (c_4)^3\}, \tag{A·1}$$

where e denotes the identity, and c_4 denotes the rotation around the z-axis by 90 degrees. It has four one-dimensional irreducible representations, i.e., A, B, E_1 and

Table II. A decomposition for a product of two irreducible representations, $R_1 \otimes R_2$, into irreducible representations in $SO(3,\mathbb{Z})$. Note that $R_1 \otimes R_2 = R_2 \otimes R_1$ by definition.

	A_1	A_2	E	T_1	T_2
A_1	A_1	A_2	E	T_1	T_2
A_2	A_2	A_1	E	T_2	T_1
E	E	E	$A_1 \oplus A_2 \oplus E$	$T_1 \oplus T_2$	$T_1 \oplus T_2$
T_1	T_1	T_2	$T_1 \oplus T_2$	$A_1 \oplus E \oplus T_1 \oplus T_2$	$A_2 \oplus E \oplus T_1 \oplus T_2$
T_2	T_2	T_1	$T_1 \oplus T_2$	$A_2 \oplus E \oplus T_1 \oplus T_2$	$A_1 \oplus E \oplus T_1 \oplus T_2$

Table III. Representation matrices of irreducible representations of C_4.

	e	c_4	$(c_4)^2$	$(c_4)^3$
A	1	1	1	1
B	1	-1	1	-1
E_1	1	i	-1	$-i$
E_2	1	$-i$	-1	i

Table IV. Numbers of each representation of C_4 which appear in each representation of $SO(3,\mathbb{Z})$.

	A	B	E_1	E_2
A_1	1	0	0	0
A_2	0	1	0	0
E	1	1	0	0
T_1	1	0	1	1
T_2	0	1	1	1

E_2. They are related to the irreducible representations of $SO(2,\mathbb{R})$ labeled by $M = 0, 2, +1, -1$ (modulo 4), respectively. The representation matrices are summarized in Table III. A relation of irreducible representations between C_4 and $SO(3,\mathbb{Z})$ is given in Table IV.

Appendix B
—— *A Source Operator for the* $^1D_2$ *State* ——

A general projection formula for the source operator in the spin singlet sector is given by

$$\mathcal{J}^{S=0;\Gamma,M}(f^{(0)}) \equiv \frac{d_\Gamma}{24} \sum_{\mathcal{R}\in SO(3,\mathbb{Z})} D^{(\Gamma)*}_{MM}(\mathcal{R}) \mathcal{J}_{\alpha\beta}(\mathcal{R}^{-1} \circ f^{(0)}) \cdot P^{(S=0,S_z=0)}_{\alpha\beta}, \qquad \text{(B·1)}$$

where Γ labels the cubic group representations (A_1, A_2, T_1, T_2, E), d_Γ denotes the dimension of the representation Γ, $D^{(\Gamma)}(\mathcal{R})$ denotes the representation matrix of the representation Γ, and M is a label of the irreducible representations of C_4, contained in the irreducible representation Γ of $SO(3,\mathbb{Z})$. (See Table IV.) This M corresponds to the azimuthal quantum number up to modulo 4 due to the cubic symmetry.

To derive Eq. (3·15), we consider the subgroup H in $SO(3,\mathbb{Z})$, which leaves $f^{(0)}(\boldsymbol{r})$ invariant

$$H \equiv \{\mathcal{R} \in SO(3,\mathbb{Z}) | \mathcal{R} \circ f^{(0)} = f^{(0)}\}. \qquad \text{(B·2)}$$

H is generated by c_2, which corresponds to the rotation around $\boldsymbol{m} \equiv (1,-1,0)$ by 180 degrees, and by c_3, which corresponds to the rotation around $\boldsymbol{n} \equiv (1,1,1)$ by 120 degrees. H consists of six elements, i.e., $H \equiv \{e, c_3, (c_3)^2, c_2, c_2c_3, c_2(c_3)^2\}$, where e denotes the identity. We decompose $SO(3,\mathbb{Z})$ by right cosets of H as $SO(3,\mathbb{Z}) = \bigcup_{c\in C_4} Hc$, where $Hc \equiv \{hc | h \in H\}$ denotes a right coset of H in G, which can be labeled by elements of C_4. We use the coset decomposition to arrange the summation in Eq. (B·1) as

$$\begin{aligned}
&\mathcal{J}^{S=0;\Gamma,M}(f^{(0)}) \\
&= \frac{d_\Gamma}{24} \sum_{c\in C_4} \sum_{h\in H} D^{(\Gamma)*}_{MM}(hc) \mathcal{J}_{\alpha\beta}((hc)^{-1} \circ f^{(0)}) \cdot P^{(S=0,S_z=0)}_{\alpha\beta} \\
&= \sum_{M'} \frac{d_\Gamma}{6} \sum_{h\in H} D^{(\Gamma)*}_{MM'}(h) \cdot \frac{1}{4} \sum_{c\in C_4} D^{(\Gamma)*}_{M'M}(c) \mathcal{J}_{\alpha\beta}(c^{-1} \circ f^{(0)}) \cdot P^{(S=0,S_z=0)}_{\alpha\beta}, \quad \text{(B·3)}
\end{aligned}$$

where we used $h^{-1} \circ f^{(0)} = f^{(0)}$. Equation (3·15) is arrived at by noting the following three facts (i) $D^{(\Gamma)*}_{M'M}(c)$ is diagonal, which reduces to a phase factor $e^{iMj\pi/2}\delta_{M'M}$, (ii) $f^{(j)} = (c_4)^{-j} \circ f^{(0)}$, where c_4 denotes the rotation around the z-axis by 90 degrees, (iii) $\frac{d_\Gamma}{6} \sum_{h\in H} D^{(\Gamma)*}_{MM}(h) = 1$ for $\Gamma = A_1$ and T_2.

References

1) R. Machleidt, Phys. Rev. C **63** (2001), 024001.
2) R. B. Wiringa, V. G. J. Stoks and R. Schiavilla, Phys. Rev. C **51** (1995), 38.
3) V. G. J. Stoks, R. A. M. Klomp, C. P. F. Terheggen and J. J. de Swart, Phys. Rev. C **49** (1994), 2950.
4) N. Ishii, S. Aoki and T. Hatsuda, Phys. Rev. Lett. **99** (2007), 022001, nucl-th/0611096.
5) S. Aoki, T. Hatsuda and N. Ishii, Prog. Theor. Phys. **123** (2010), 89, arXiv:0909.5585; Comput. Sci. Dis. **1** (2008), 015009, arXiv:0805.2462.
6) H. Nemura, N. Ishii, S. Aoki and T. Hatsuda, Phys. Lett. B **673** (2009), 136, arXiv:0806.1094.
7) T. Inoue et al. (HAL QCD Collaboration), Prog. Theor. Phys. **124** (2010), 591, arXiv:1007.3559.
8) T. Inoue et al. (HAL QCD Collaboration), arXiv:1012.5928.
9) T. Doi for HAL QCD Collaboration, arXiv:1011.0657.
10) Y. Ikeda et al. (HAL QCD Collaboration), arXiv:1002.2309.
11) T. Kawanai and S. Sasaki, Phys. Rev. D **82** (2010), 091501, arXiv:1009.3332.
12) S. Aoki, J. Balog and P. Weisz, Prog. Theor. Phys. **121** (2009), 1003, arXiv:0805.3098.
13) K. Murano, N. Ishii, S. Aoki and T. Hatsuda, PoS(Lattice 2010)150, arXiv:1012.3814.
14) K. Murano, N. Ishii, S. Aoki and T. Hatsuda, PoS(LAT2009)126, arXiv:1003.0530.
15) M. Luscher, Commun. Math. Phys. **105** (1986), 153.
16) M. Luscher, Nucl. Phys. B **354** (1991), 531.
17) C. J. D. Lin, G. Martinelli, C. T. Sachrajda and M. Testa, Nucl. Phys. B **619** (2001), 467, hep-lat/0104006.
18) S. Aoki et al. (CP-PACS Collaboration), Phys. Rev. D **71** (2005), 094504, hep-lat/0503025.
19) N. Ishizuka, PoS(LAT2009)119, arXiv:0910.2772.
20) W. Królikowski and J. Rzewuski, Nuovo Cim. **4** (1956), 1212.
21) S. Okubo and R. E. Marshak, Ann. of Phys. **4** (1958), 166.
22) R. Tamagaki and W. Watari, Prog. Theor. Phys. Suppl. No. 39 (1967), 23.
23) M. Fukugita, Y. Kuramashi, M. Okawa, H. Mino and A. Ukawa, Phys. Rev. D **52** (1995), 3003.
24) N. Ishii et al. (HAL QCD Collaboration), in preparation.
25) CPS++, `http://qcdoc.phys.columbia.edu/cps.html` (maintainer: Chulwoo Jung).

26) E. P. Wigner, *Group Theory and Its Application to the Quantum Mechanics of Atomic Spectra*, expanded and improved ed. (Academic Press, New York, 1971).
27) L. D. Landau and L. M. Lifshitz, *Quantum Mechanics (Non-relativistic Theory)*, 3rd ed. (Butterworth-Heinemann, New York, 1977).